Cronfa - Swansea University Open Access Repository

This is an author produced version of a paper published in :
Journal of Applied Physics

Cronfa URL for this paper:
http://cronfa.swan.ac.uk/Record/cronfa21324

Paper:

Barnett, C., Kryvchenkova, O., Wilson, L., Maffeis, T., Kalna, K. & Cobley, R. (2015). The role of probe oxide in local surface conductivity measurements. *Journal of Applied Physics, 117*(17), 174306

http://dx.doi.org/10.1063/1.4919662

This article is brought to you by Swansea University. Any person downloading material is agreeing to abide by the terms of the repository licence. Authors are personally responsible for adhering to publisher restrictions or conditions. When uploading content they are required to comply with their publisher agreement and the SHERPA RoMEO database to judge whether or not it is copyright safe to add this version of the paper to this repository.
http://www.swansea.ac.uk/iss/researchsupport/cronfa-support/

The role of probe oxide in local surface conductivity measurements

C. J. Barnett[1], O. Kryvchenkova[1], L. S. J. Wilson[1], T. G. G. Maffeis[1], K. Kalna[2] and R. J. Cobley[1]

1 Multidisciplinary Nanotechnology Centre, College of Engineering, Swansea University, Singleton Park, Swansea SA2 8PP, U.K.

2 Electronic Systems Design Centre, College of Engineering, Swansea University, Singleton Park, Swansea SA2 8PP, U.K.

ABSTRACT

Local probe methods can be used to measure nanoscale surface conductivity, but some techniques including nanoscale four point probe rely on at least two of the probes forming the same low resistivity non-rectifying contact to the sample. Here, the role of probe shank oxide has been examined by carrying out contact and non-contact I V measurements on GaAs when the probe oxide has been controllably reduced, both experimentally and in simulation. In contact the barrier height is pinned but the barrier shape changes with probe shank oxide dimensions. In non-contact measurements, the oxide modifies the electrostatic interaction inducing a quantum dot that alters the tunneling behavior. For both, the contact resistance change is dependent on polarity, which violates the assumption required for four point probe to remove probe contact resistance from the measured conductivity. This has implications for all nanoscale surface probe measurements and macroscopic four point probe, both in air and vacuum, where the role of probe oxide contamination is not well understood.

This is the accepted version of the following article:

J. Appl. Phys. 117, 174306 (2015); http://dx.doi.org/10.1063/1.4919662

which has been published in final form at

http://scitation.aip.org/content/aip/journal/jap/117/17/10.1063/1.4919662

Copyright for the published version resides with the American Institute of Physics

I. INTRODUCTION

A number of probe based techniques have been developed to measure nanoscale surface conductivity [1]. Scanning tunneling spectroscopy (STS) uses one probe to measure surface conductivity by measuring the current tunneling between the probe and a grounded sample. However, STS is mainly dependent on transport though the tunneling junction, rather than the underlying properties of the material, although the junction formed is indicative of those material properties. Two point probe measurements can be used to measure nanoscale conductivity but are also dependent on the contact resistance caused by the barrier formation and the resistance of the wires connecting the probes. In three probe measurements, a current is passed through the two outer probes and a third scanning tunneling microscopy (STM) probe is used to map the potential at the surface. Three point probe measurements can mimic and have the advantages of four point probe measurements. However, the scan range of an STM is usually very small and so is the potential change between different points on a surface [1]. Finally, collinear four point probe employs two outer probes to pass a current through the sample while two inner high impedance sense probes measure the potential difference induced by the outer probes[2].

Despite the wide use of four point probe methods, there exists disagreement in the literature about whether the contact type of the four probes is important. While some claim the measurements are independent of contact and wire resistances regardless of the probe-sample contact type [1, 3-6], others have found that four point probe measurements will not give accurate results if the contact type is Schottky [2, 7-10]. In order to address this, a short review of four point probe is presented and a model to describe the system is developed.

The first formalism for the collinear four point probe with an equal probe spacing, *s*, was introduced by Valdes [3] in 1954 with the equation for the resistivity, *ρ*, when probes are placed on a semi-infinite volume of semiconductor material given as:

$$\rho = 2\pi s \cdot V/I \tag{1}$$

where *I* is current and *V* is voltage. For other probe geometries and spacing, correction factors are used to allow a similar treatment [11]. The most common experimental setup is the collinear mode as shown in FIG. 1 [1, 2, 5] where probes 1 and 4 are used for current sensing and probes 2 and 3 are used for voltage sensing.

A model of four point probe and its connection to the instrumentation is constructed here in FIG. 1(b) based on an instrument connection model presented by Keithley [9] using resistance contributions shown explicitly by Sohn [12] and discussed elsewhere by Keithley [8]. In this model, each probe has a probe resistance R_p, a contact resistance R_{cp} at the probe-sample contact, a spreading resistance R_{sp} due to the current flowing from the probe through the sample, and the semiconductor itself has a sheet resistance R_s which needs to be measured. Ideally contact resistance, probe (lead) resistance, and spreading resistance (R_{cp}, R_p, and R_{sp}) should not contribute to the measurement of the sheet resistance R_s.

In the collinear four point probe method the inner two probes will draw negligible current from the sample due to the high impedance of the voltmeter used in the measurements. This will result in very low current through the inner voltage probes 2 and 3 making $I_2 \ll I_1$ and $I_3 \ll I_4$. Unlike in two point probe measurements[13], this explains why the contact type (Schottky or Ohmic) of the voltage probes in four point probe does not play a significant role [3]. Due to negligible current I_2 and I_3, the voltage V measured by the voltmeter will correspond to the potential drop across the sample V_s making: $V = V_s$. Also, when the current through the voltage probes is negligible, the current through probes 1 and 4 becomes: $I_1 = I_s = I_4$ as seen in Figure 1.1.2(b). Then the measured resistance using four point probe is:

$$R_s = {}^{V}\!/_{I_1} = {}^{V_s}\!/_{I_s} \qquad (2)$$

Many authors also claim that the contact type of the current probes (probes 1 and 4 in FIG. 1(a)) do not influence four point probe measurements, irrespective of whether the probe-sample contacts are Ohmic or Schottky [1, 4-6]. Some authors cite Smits' work [11] from 1958 to confirm the assumption even though this work does not include a study of the probe contact type.

The condition of rectifying contacts appearing in four point probe was addressed by Valdes [3] in 1954 to study the surface resistivity of germanium. Valdes derived the formulism to improve the existing measurement methods, claiming the new four point probe method accounted for the rectifying nature of the contact formed between the germanium semiconductor and the metal probe [3]. Excess concentrations of minority carriers were known to affect the potential of contacts and it was claimed to modulate the resistance of the material [3]. It is now widely accepted that resistance (resistivity) is an intrinsic property of the material independent of the

measurement method [14] and it cannot be modulated by the properties of the contact; instead the contact resistance can introduce an error in the measurement of the semiconductor resistivity. Valdes' formulism did not account for the separate impact of contact resistance and material resistivity, and a semiconductor sample was considered to be a semi-infinite volume of uniform resistivity material [3].

Valdes in Ref. [3] is referencing work by Bardeen [15] which demonstrates non-linear current-voltage behavior of germanium point contacts. It is now known that in Schottky contacts there are five basic transport processes [14, 16-18],: (1) emission of electrons from the semiconductor over the potential barrier into the metal, (2) quantum-mechanical tunneling of electrons through the barrier (important for heavily doped semiconductors and responsible for most Ohmic contacts), (3) recombination in the space-charge region, (4) diffusion of electrons in the depletion region, and (5) holes injected from the metal that diffuse into the semiconductor. Current due to each transport process takes place at different bias ranges and its dependence on the applied bias is non-linear. This means that in Schottky contacts, the current in to the electrode and out of the electrode will have significantly different magnitudes for a set voltage magnitude of alternate polarity. If we consider that current probes 1 and 4 in FIG. 1(a) have the same material parameters and both probes are forming Schottky contacts with the sample, then for the current directions indicated in FIG. 1(a) the forward bias current I_1 and corresponding reverse bias current I_4 are non-equal ($I_1 \neq I_4$) and form contact resistances: $R_{cp1} << R_{cp4}$. This would violate one of the main principles of four point probe theory: current-carrying electrodes carry currents of equal magnitude but in opposite directions [3]. This rise of the contact resistance R_{cp1} or R_{cp4} will result in non-negligible current through the voltage probes I_2 and I_3, causing $V \neq V_s$, which then results in the same measurement errors as seen in two point probe.

Experimental data demonstrated by Chandra [10] indicated that for the wide band gap semiconductor SiC, four point probe measurements are not suitable, even though it is routinely used for Si and other semiconductors. One probe measurements on the SiC surface revealed the non-linear current-voltage characteristic. Extremely high contact resistances for the probe–SiC contacts were estimated using four point probe [10]. This was due to high current through the voltage probes (probes 2 and 3 FIG. 1(a)) in comparison to the current through the actual current probes (1 and 4 in FIG. 1(a)). Therefore problems arise when measuring sheet resistance with the four-point probe method on SiC surfaces with non-linear I-V characteristics [10]. These measurements demonstrate that for the case of non-Ohmic contacts, a violation of one of the principles of four point probe

formulism is present: the current on the voltage probes becomes non-negligible in comparison to the current through the current probes.

It is recommended by four point probe instrumentation companies to make one probe measurements to test whether the current-voltage behavior is linear before the measurement, and successful four point probe measurements demonstrated in the literature are performed with Ohmic probe-sample contacts [5, 8, 9, 12, 13, 19-21]. Hesse [7] also states that conventional four point probe measurement methods are unsuitable if Schottky behavior occurs between the metallic contact and the sample.

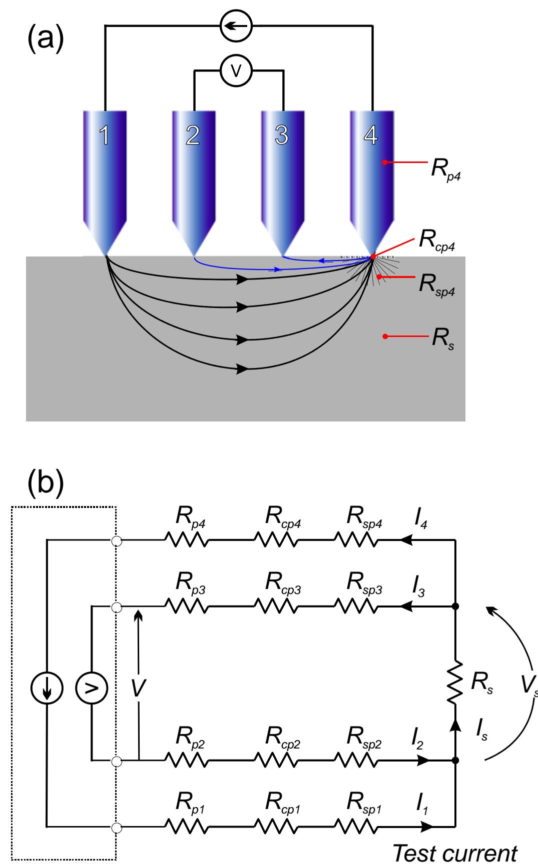

FIG. 1. (Color online) Four point probe measurements of semiconductor resistance. (a) The outer two probes 1 and 4 are used for supplying current while the inner two probes 2 and 3 are used for voltage sensing. Each probe has a probe resistance R_P, at the probe-sample contact there is a contact resistance R_{cp}, spreading resistance R_{sp}, and semiconductor itself has a sheet resistance R_s. (b) Current from the voltage probes 2 and 3 is negligible when a voltmeter has high impedance: $I_2 << I_1$, $I_3 << I_4$, $I_1 = I_s = I_4$. Then the voltage sensed by voltmeter (V) will be equal to the voltage drop across the sample: $V = V_s$. The measured resistance becomes: $R_s = V/I_1 = V_s/I_s$.

With the need for Ohmic contacts established, even for four point probe, we now turn our attention to whether oxide coatings on local probes can modify the contact behavior. Oxide coatings can have an effect on the contact type formed, and so four point probe measurements should be taken with probes that are oxide free using methods such as direct current annealing [9, 22]. Li and Ba state that the probes used for four point probe measurement need to be regularly cleaned to avoid the effect of probe surface oxidation and/or contamination, but as of 2012 they report that no work has been done to examine the effects of probe oxide [2].

For STS, Gimzewski [23], observed that leaving an iridium probe to degrade in ultra-high vacuum (UHV) changed the spectrum of a silver sample from Ohmic to Schottky, suggesting carbon or oxygen contamination of the probe. Studies carried out by Shen and Clemens show the effect on the STS spectra when a layer of indium oxide is deposited on InGaAs [24, 25]. Both studies noted that the band edges shifted down in energy when a monolayer of In_2O was deposited on n-type InGaAs and only the conduction band (CB) edge shifted towards the Fermi level when p-type InGaAs was used. Shen suggests that this behavior is due to surface band bending caused by surface dipoles or surface states.

Most of this work assumes that the oxide forms a layer between the probe and sample, but in this paper we find that even if such a layer is removed, residual oxide on the probe shank can alter the contact behavior. Previous work has shown that cleaning probes by direct current annealing will not remove all of the oxide [26]. Here we examine the effects of probe shank oxide layers on the probe-sample contact type by taking contact and non-contact measurements with the probe shank oxide in place and controllably reduced. Both tunneling and thermionic emission can play a role in contact measurements. To separate the contributions and study them in relative isolation, both contact and non-contact measurements are studied. Simulations and experimental results find that although the barrier height is fixed in contact measurements, the probe shank oxide modifies the electrostatic interaction which changes the barrier shape non-equally for current transport in and out. For non-contact tunneling, we find that the barrier height is modified by the amount of probe shank oxide, again differently for current tunneling in compared to tunneling out. For both cases the apex of the probe is free of oxide to allow tunneling or contact transport. Although this is a local process, the long-range electrostatic interaction from further up the probe shaft modifies the background structure into which the transport takes place.

II. METHOD

Probes were electrochemically etched from 0.25 mm diameter polycrystalline tungsten wire in 2M KOH in a method similar to Ibe [27]. The tungsten to oxygen ratio (W:O) was measured to verify the controllable reduction of surface oxide by calibrated direct current annealing using an Hitachi S-4800 field emission scanning electron microscope (SEM) with an Oxford Instruments X-Max 50 analyzer for energy-dispersive X-ray spectroscopy (EDX) [26]. Probes which did not reproducibly clean or were observed with SEM to have crashed when checked after measurement were rejected. N-type GaAs doped 9.2×10^{17} cm^{-3} with Zn was cleaved in UHV to expose an atomically flat (110) surface [28]. For each sample, one hundred I-V or spectroscopy curves were collected at room temperature in a ten by ten grid and averaged to produce each spectrum. To ensure that the probe properties did not change during the measurements, all spectra and image properties were monitored in the scan direction, and only complete sets where the probe did not undergo change during the scan were used. The non-contact case was repeated 4 times and the contact case was repeated twice, the same trends were found in all repeats. For non-contact measurements, results were found to be dependent on doping concentration therefore results for GaAs, doped 1.7×10^{16} cm^{-3} with Zn are also presented.

For contact measurements, the feedback loop was disabled at the 0.5 nA set point and the probe approached incrementally by dz = 0.1 nm until the spectroscopy was observed to change from tunneling dominated to contact dominated. This occurred at dz = –0.5 nm and was used for all contact measurements. For non-contact measurements, the feedback loop was enabled for a current set point of 0.1 nA which maintained constant separation.

The principle oxide found on a tungsten probe after electrochemical etching is WO_3, which is a wide band gap semiconductor, and for un-cleaned probes if tunneling was taking place through the oxide at the probe apex, the WO_3 band structure would convolve with the sample band structure to produce spectra with a much wider apparent band gap. This is the opposite of what we observe experimentally, and later we will show that the probe apex behaves predominantly as a metal. Therefore, we find that during the initial probe approach the probe moves close enough to the sample surface to mechanically remove the oxide coating, before tunneling initiates through the exposed metal probe apex. Direct current annealing at 1714 K is high enough to sublimate the oxide and is low enough to prevent blunting of the probe, but a residual oxide layer remains [26]. In line with this, and our SEM and EDX results, we construct a model of a 32 nm diameter probe with a 1 nm WO_3 layer

around the shank of the probe. After annealing the probe shaft oxide is reduced to 0.3 nm, with the probe apex exposed for both. This structure used for all simulations is shown in FIG. 2.

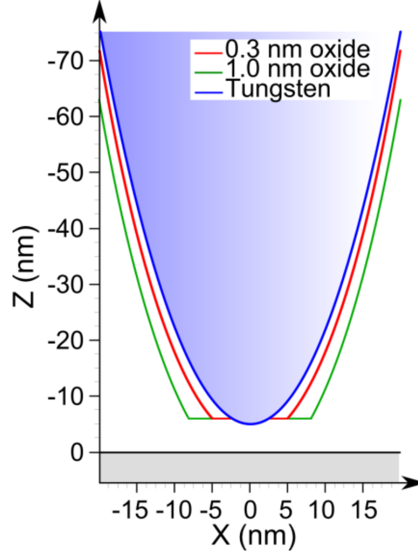

FIG. 2. (Color online) Physical model of the probe, with an exposed metal apex and oxide coated shaft.

The 2D structure of the probe-sample system was modelled within the simulation tool Atlas [29-32]. The carrier transport model uses a drift-diffusion approximation for the GaAs sample assuming semi-infinite geometry, incorporating tunneling between the tip and the sample which is self-consistently coupled with Poisson's equation, thus accounting for long-range Coulomb interactions.

The tunneling current contributing to drift and diffusion currents was calculated using a direct quantum tunneling model by Tsu and Esaki [33, 34] which accounts for the tunneling through a very thin air gap (<1 nm). The tunnelling current density J through a potential barrier is obtained according to the following formula:

$$\mathrm{J} = \frac{qkT}{2\pi^2\hbar^3} m^* \int T(E) \times ln\left[\frac{1+e^{(E_{Fsamp}-E)/kT}}{1+e^{(E_{Ftip}-E)/kT}}\right] \tag{3}$$

where $T(E)$ is the transmission probability, $m^* = \sqrt{m_x m_y}$ (where m_x and m_y are carrier effective masses in the lateral directions), E is the charge carrier energy, $E_{F_{tip}}$ is the probe quasi-Fermi level, $E_{F_{samp}}$ is the sample quasi-Fermi level, q is the electron charge, k is Boltzmann constant, T is temperature and ħ is the reduced Planck's constant. At every bias point, the band edge position is determined and used in the calculation of the integration term making tunnelling current J equal to zero at the equilibrium $\left(E_{F_{samp}} = E_{F_{tip}}\right)$. The transmission

probability $T(E)$ was calculated according to the Gundlach formula for a trapezoidal potential barrier [35] with both the incident and transmitted currents. Schrödinger's equation was solved in the effective mass approximation [36]. Homogeneous (reflecting) Neumann boundary conditions were used for the non-contact areas while Dirichlet boundary conditions were used for the tungsten probe and the sample contact.

When an STM probe is in contact with the semiconductor surface and a Schottky contact is formed there are two principle current transport mechanisms: thermionic emission of carriers over the potential barrier and tunneling through the potential barrier. In the model, the potential barrier height at the metal-semiconductor interface is calculated from the standard expression of the Schottky-Mott theory [37]. The field dependent barrier lowering due to the image force $\Delta\phi_{im}$ is included in the simulation as follows [17]:

$$\Delta\phi_{im} = \sqrt{qE/4\pi\varepsilon_s} \quad (4)$$

where ε_S is the permittivity of the semiconductor. When incorporating the thermionic emission model, the surface thermal velocities for electrons (holes) V_S were calculated as follows [38]:

$$V_s = A_R T^2 / qN_c \quad (5)$$

where A_R is the effective Richardson constants for electrons (holes) and N_C is the effect density of states in the conduction band

The electron (hole) J_{th} current at the surface due to thermionic emission is calculated using the electric field at each mesh point of the structure, taking into account the barrier lowering terms $\Delta\phi_b = \phi_b - \Delta\phi_{im}$:

$$J_{th} = qV_s(n_s - n)e^{\Delta\phi/kT} \quad (6)$$

where n_s is the surface concentration of electrons (holes) and n is the concentration of electrons (holes).

The universal Schottky tunneling model is used to estimate the tunneling current J_{tunn} through the Schottky barrier, where the localized tunneling rates are calculated close to the metal-semiconductor interface for both electrons and holes [39, 40] as follows:

$$J_{tunn} = \frac{A_R T}{k} \int_0^\infty \Gamma(E) ln\left(\frac{1+f_s(E)}{1+f_m(E)}\right) dE \quad (7)$$

Where $\Gamma(E)$ is the tunnelling probability, $f_s(E)$ and are $f_m(E)$ Maxwell-Boltzmann distribution functions in semiconductor and metal. The tunneling probability is calculated using the Wentzel-Kramers-Brillouin (WKB) method assuming a linear variation of the potential between two mesh points.

Mid band gap surface states could be accounted for in this model, but the *in situ* cleaved atomically flat (110) surface of GaAs contains no surface state distributions centered in the band gap and so they were not included.

III. RESULTS

A. Contact

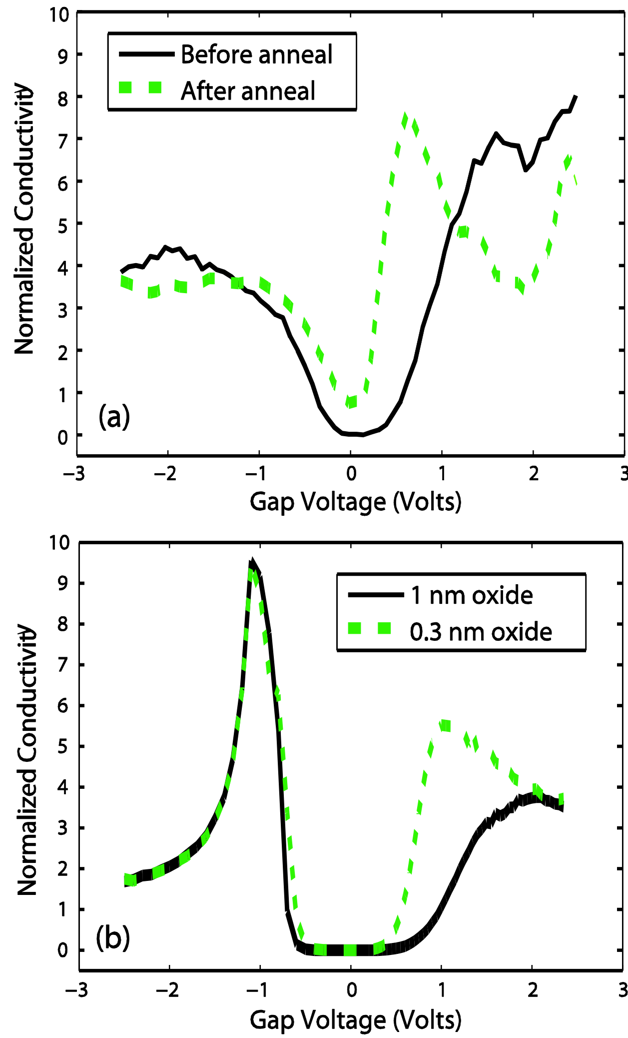

FIG. 3. (Color online) Normalized conductivity as a function of applied bias with a denominator offset constant $c = 0.02$ and a rolling average of six for contact measurements on GaAs (a) experimental and (b) simulation.

Experimental and simulated measurements of normalized conductivity for the contact case on GaAs are shown in FIG. 3. Normalized conductivity is an invariant quantity that indicates features of surface state distributions and is calculated using the following equation [41]:

$$\frac{dI/dV}{\sqrt{(I/V)^2 + c^2}} \tag{8}$$

where c is a small offset to prevent divergence as the denominator goes towards zero [42].

The conductivity both experimentally and in simulation increases after the probe shank oxide is reduced. The simulations and experimental results contain the same features with quantitative agreement. Discrepancies arise from the probe geometry estimated from SEM images and non-uniform oxide formation which was modelled as uniform. Simulations find that the creation of a near-intimate contact between the probe and sample forms a Schottky contact with a fixed barrier height for both. However, the different shank oxide profile before and after cleaning alters the electrostatic interaction with the sample, changing the shape and width of the barrier, giving rise to the altered transport shown. Importantly, the change for electron transport into the sample (positive gap voltage), where the presence of the Schottky contact means tunneling dominates, is much more pronounced than the change observed for electron transport out of the sample (negative gap voltage), where thermionic emission dominates. This result confirms that the barrier for current into and out of the sample for probes in the four point probe method would be unequally affected by probe shank oxide, and could lead to a violation of the assumptions which make four point probe measurements independent of contact resistance.

B. Non-contact

For the high doped sample shown in FIG. 4(a), the electron transport in (positive gap voltage) is observed to shift after probe shank oxide removal, where simulations find that the probe field is high enough to induce localized surface depletion creating a probe-induced quantum dot with empty discrete states in the valance band (VB) above the Fermi level. An example is shown in FIG. 5, where at +1.8 V for the highly doped sample, localized band bending is larger with the thicker probe oxide before annealing. This leads to discrete states above the Fermi level in the VB which the probe electrons tunnel in to before the voltage is high enough to tunnel in to the conduction band (CB). Thermal broadening, where the Fermi function is non-abrupt at room temperature, means the additional states are not resolved individually but still add to the overall current.

For low doped GaAs, these long range electrostatic interactions are essentially already so high that there is little difference when the probe oxide is changed. The only exception is a shoulder centered around 1 V caused by the on-set of the quantum dot, which appears earlier when the probe oxide has not been reduced. Both experimental and simulated results show the same effect.

In all non-contact cases both the experimental data and the model show that electron tunneling does not shift significantly after probe annealing. With negative gap voltage, the sample is in accumulation and the screening effects of the dopants reduce the electrostatic probe-induced band bending.

A similar shift in the spectra observed by Shen and Clemens may be due to a similar effect as that observed here [24, 25]. In their case, the oxide layer deposited on the InGaAs sample reduces the effect of the electric field and reduces the probe induced band bending which causes the CB edge to shift towards the Fermi level.

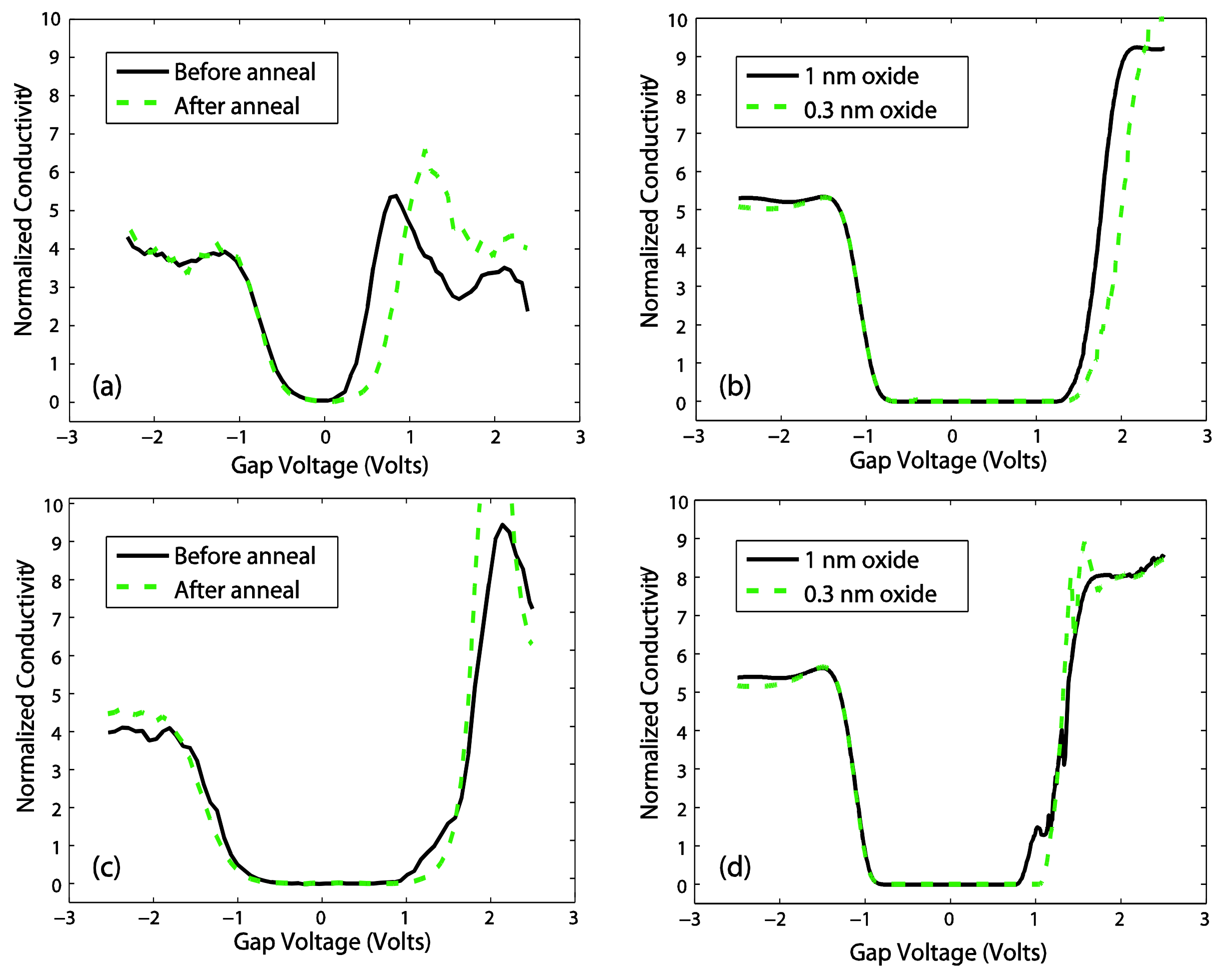

FIG. 4. (Color online) Normalized conductivity versus gap voltage (sample bias) with a denominator offset constant c = 0.02 and a rolling average of six for non-contact measurements on highly doped GaAs (a) experimental and (b) simulation and low doped GaAs (c) experimental and (d) simulation.

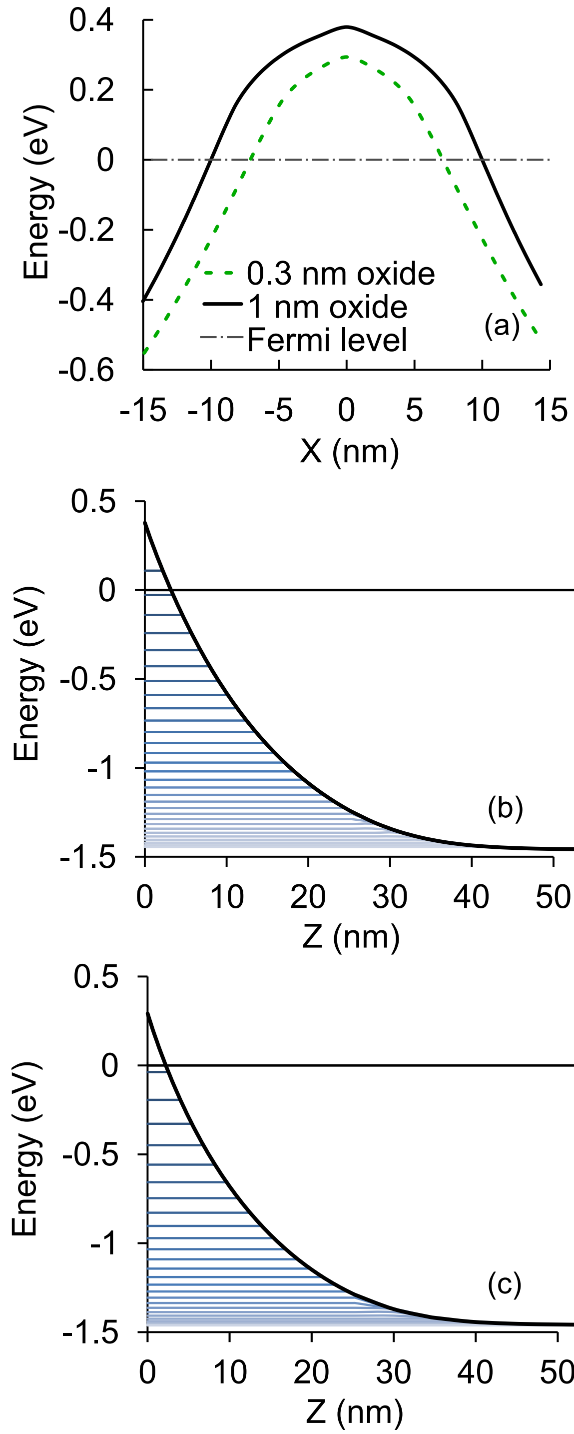

FIG. 5. (Color online) For highly doped GaAs at +1.8 V gap voltage with a non-contact probe, simulations show (a) VB profile along the sample surface at z =0 under the probe in the x-direction, before and after annealing (solid and dashed lines respectively) with the VB profile under the probe at x=0 in to the sample in the z direction (b) before probe annealing and (c) after annealing. All plots use the Fermi level as 0 and are consistent with the spatial directions established in FIG. 2, with discrete states shown as horizontal lines within the VB in (b) and (c).

IV. CONCLUSION

The presence of oxide on probes used for local conductivity measurements of semiconductors has been investigated experimentally and in simulation. For contact measurements the presence of oxide on the shank of the probe alters the contact behavior with the resulting current transport dependent on the voltage polarity. When injecting electrons into the sample, the presence of shank oxide causes a widening of the Schottky barrier which does not occur when removing electrons from the sample. This results in non-equal resistivity in and out of the sample when carrying out contact measurements when the shank oxide is present. This also means that the increased size of the Schottky barrier increases the resistance of the contact when the probe oxide is present. Both of these results confirm that the assumption contact type is irrelevant in four point probe measurements is violated.

When in the non-contact regime, the main shifts in the spectra occur when the sample is in depletion, where a tip-induced quantum dot is created in the sample below the probe. The shape and size of the induced quantum dot is altered by the electrostatic field from the tip, which is governed by the oxide coating. When an oxidized probe is used, the resulting tip-induced quantum dot causes empty discrete states above the Fermi level in the VB which results in increased tunneling. When the oxide coating is reduced, the smaller tip induced quantum dot does not create discrete states above the Fermi level. A similar shift in the spectra observed by Shen and Clemens may be due to a similar effect as that observed here [24, 25]. In their case, the oxide layer deposited on the InGaAs sample reduces the effect of the electric field and reduces the tip induced band bending which causes the CB edge to shift towards the Fermi level.

In summary, this work has implications for all nanoscale surface probe measurements and macroscopic four point probe, both in air and vacuum, when probe shank oxide may be present even after annealing.

ACKNOWLEDGMENTS

This work was part funded by the EPSRC studentship and the RCUK.

REFERENCES

1. P. Hofmann and J. W. Wells, Journal of Physics: Condensed Matter **21** (1), 013003 (2009).
2. J. C. Li, Y. Wang and D. C. Ba, Physics Procedia **32** (0), 347-355 (2012).
3. L. B. Valdes, Proceedings of the IRE **42** (2), 420-427 (1954).
4. A.-P. Li, K. W. Clark, X. G. Zhang and A. P. Baddorf, Advanced Functional Materials **23** (20), 2509-2524 (2013).
5. J. W. Wells, J. F. Kallehauge and P. Hofmann, Surface Science **602** (10), 1742-1749 (2008).
6. S. Hasegawa and F. Grey, Surface Science **500** (1–3), 84-104 (2002).
7. E. Hesse, Instrumentation and Measurement, IEEE Transactions on **IM-31** (3), 166-175 (1982).
8. Keithley Appl. Note Ser. **no. 2481**.
9. P. Foster and J. Hochbert, (2004), Vol. 2014.
10. N. Chandra, V. Sharma, G. Y. Chung and D. K. Schroder, Solid-State Electronics **64** (1), 73-77 (2011).
11. F. M. Smits, Bell System Technical Journal **37** (3), 711-718 (1958).
12. S. Sohn and H.-M. Kim, *Transparent Conductive Oxide (TCO) Films for Organic Light Emissive Devices (OLEDs)*. (2011).
13. S. Yoshimoto, Y. Murata, K. Kubo, K. Tomita, K. Motoyoshi, T. Kimura, H. Okino, R. Hobara, I. Matsuda, S.-i. Honda, M. Katayama and S. Hasegawa, Nano Letters **7** (4), 956-959 (2007).
14. S. Dimitrijev, *Principles of Semiconductor Devices*. (Oxford University Press, New York, 2006).
15. J. Bardeen, Bell System Technical Journal **29** (4), 469-495 (1950).
16. C. R. Crowell and S. M. Sze, Solid-State Electronics **9** (11–12), 1035-1048 (1966).
17. S. M. Sze and K. K. Ng, *Physics of Semiconductor Devices*. (Wiley, 2006).
18. R. T. Tung, Materials Science and Engineering: R: Reports **35** (1–3), 1-138 (2001).
19. C. de Saint-Aubin, M. El Hajj Hassan, P. Kunemann, T. Patois, B. Lakard, R. Fabre, J. Hemmerlé, P. Schaaf, M. Nardin and M.-F. Vallat, Synthetic Metals **194** (0), 38-46 (2014).
20. C. Durand, M. Berthe, Y. Makoudi, J.-P. Nys, R. Leturcq, P. Caroff and B. Grandidier, Nanotechnology **24** (27), 275706 (2013).
21. B.-F. Ju, Y. Ju and M. Saka, Journal of Micromechanics and Microengineering **15** (12), 2277 (2005).
22. A. S. Lucier, H. Mortensen, Y. Sun and P. Grutter, Physical Review B **72** (23) (2005).
23. J. K. Gimzewski and R. Möller, Physical Review B **36** (2), 1284-1287 (1987).
24. J. Shen, E. A. Chagarov, D. L. Feldwinn, W. Melitz, N. M. Santagata, A. C. Kummel, R. Droopad and M. Passlack, Journal of Chemical Physics **133** (16) (2010).
25. J. B. Clemens, E. A. Chagarov, M. Holland, R. Droopad, J. Shen and A. C. Kummel, Journal of Chemical Physics **133** (15) (2010).
26. R. J. Cobley, R. A. Brown, C. J. Barnett, T. G. G. Maffeis and M. W. Penny, Applied Physics Letters **102** (2) (2013).
27. J. P. Ibe, P. P. Bey, S. L. Brandow, R. A. Brizzolara, N. A. Burnham, D. P. Dilella, K. P. Lee, C. R. K. Marrian and R. J. Colton, Journal of Vacuum Science & Technology a-Vacuum Surfaces and Films **8** (4), 3570-3575 (1990).
28. R. J. Cobley, K. S. Teng, M. R. Brown, P. Rees and S. P. Wilks, Applied Surface Science **256** (19), 5736-5739 (2010).
29. *ATLAS User's Manual*. (2007).
30. O. Kryvchenkova, R. J. Cobley and K. Kalna, Applied Surface Science **295** (0), 173-179 (2014).
31. O. Kryvchenkova, K. Kalna and R. J. Cobley, presented at the Advanced Semiconductor Devices & Microsystems (ASDAM), 2014 10th International Conference on, 2014 (unpublished).
32. O. Kryvchenkova, K. Kalna and R. J. Cobley, presented at the Conference on Advanced Nanomaterials (ANM 2014), 2014 (unpublished).
33. R. Tsu and L. Esaki, Applied Physics Letters **22** (11), 562-564 (1973).
34. P. Price and J. Radcliffe, Ibm Journal of Research and Development **3** (4), 364-371 (1959).

35. K. H. Gundlach, Solid-State Electronics **9** (10), 949-957 (1966).
36. D. K. Ferry, *Semiconductors*. (Macmillan, 1991).
37. E. H. Rhoderick, IEE Proceedings I (Solid-State and Electron Devices) **129** (1), 1-14 (1982).
38. V. L. Rideout and C. R. Crowell, Solid-State Electronics **13** (7), 993-& (1970).
39. K. Matsuzawa, K. Uchida and A. Nishiyama, Ieee Transactions on Electron Devices **47** (1), 103-108 (2000).
40. M. Ieong, P. M. Solomon, S. E. Laux, H. S. P. Wong and D. Chidambarrao, in *International Electron Devices Meeting 1998 - Technical Digest* (1998), pp. 733-736.
41. M. Prietsch, A. Samsavar and R. Ludeke, Physical Review B **43** (14), 11850-11856 (1991).
42. P. Guaino, A. A. Cafolla, O. McDonald, D. Carty, G. Sheerin and G. Hughes, Journal of Physics: Condensed Matter **15** (38), S2693 (2003).